

# Colloids and polymers in random colloidal matrices: demixing under good-solvent conditions

Mario Alberto Annunziata\*

*CNR, Istituto dei Sistemi Complessi*

*(Area della Ricerca di Roma Tor Vergata)*

*Via del Fosso del Cavaliere 100,*

*I-00133 Roma, Italy*

*e-mail: m.annunziata@isc.cnr.it*

Andrea Pelissetto

*Dipartimento di Fisica,*

*Università degli Studi di Roma “La Sapienza”*

*and INFN – Sezione di Roma I*

*Piazzale A. Moro 2,*

*I-00185 Roma, Italy*

*e-mail: Andrea.Pelissetto@roma1.infn.it*

---

\* Present address: Institut für Theoretische Physik II, Heinrich-Heine-Universität Düsseldorf, Universitätsstrasse 1, D-40225 Düsseldorf, Germany

## Abstract

We consider a simplified coarse-grained model for colloid-polymer mixtures, in which polymers are represented as monoatomic molecules interacting by means of pair potentials. We use it to study polymer-colloid segregation in the presence of a quenched matrix of colloidal hard spheres. We fix the polymer-to-colloid size ratio to 0.8 and consider matrices such that the fraction  $f$  of the volume that is not accessible to the colloids due to the matrix is equal to 40%. As in the Asakura-Oosawa-Vrij (AOV) case, we find that binodal curves in the polymer and colloid volume-fraction plane have a small dependence on disorder. As for the position of the critical point, the behavior is different from that observed in the AOV case: while the critical colloid volume fraction is essentially the same in the bulk and in the presence of the matrix, the polymer volume fraction at criticality increases as  $f$  increases. At variance with the AOV case, no capillary colloid condensation or evaporation is generically observed.

PACS numbers: 61.25.Hq, 82.35.Lr

## I. INTRODUCTION

The study of the properties of fluids in porous materials [1] is very important for its technological applications in many fields of science, from physics and chemistry to geology, engineering, and even agriculture. In this paper we consider the demixing of a binary mixture of nonadsorbing colloids of radius  $R_c$  and of polymers of radius of gyration  $R_g$ , with the purpose of understanding how the porous structure influences the phase behavior. We are considering mesoporous disordered materials, like silica gels, which present large pores and can thus adsorb mesoscopic particles like colloids. In the bulk the phase behavior of colloid-polymer mixtures depends on the parameter  $q = R_g/R_c$ . For  $q$  small,  $q < q_c$  ( $q_c \approx 0.2$ - $0.3$  under good-solvent conditions), only a fluid-solid transition is observed, analogous to that observed in hard-sphere systems. For  $q > q_c$  also a fluid-fluid transition occurs, between a colloid-liquid (polymer-poor) and a colloid-gas (polymer-rich) phase. It is such a fluid-fluid transition that will be investigated in the present paper.

At least qualitatively, many aspects of the behavior of polymer-colloid mixtures can be understood by using the Asakura-Oosawa-Vrij (AOV) model [2, 3], which gives a coarse-grained (CG) description of the mixture. Polymers are treated as an ideal gas of point particles, whose radius is identified with the radius of gyration  $R_g$ , which interact with the colloids (hard spheres of radius  $R_c$ ) by means of a simple hard-core potential. This model is extremely crude since it ignores the polymeric structure and polymer-polymer repulsion, which is relevant in the good-solvent regime. Nonetheless, it correctly predicts polymer-colloid demixing as a result of the entropy-driven effective attraction (depletion interaction) between colloidal pairs due to the presence of the polymers [4–12]. AOV colloid-polymer mixtures in a porous matrix have been studied in Refs. [13–18] by means of density-functional theory, integral equations, and Monte Carlo (MC) simulations. The nature of the critical transition has been fully clarified [14–17]: if the obstacles are random and there is a preferred affinity of the quenched obstacles to one of the phases, the transition is in the same universality class as that occurring in the random-field Ising model, in agreement with a general argument by de Gennes [19]. If these conditions are not satisfied, standard Ising or randomly dilute Ising behavior is observed instead, see Refs. [20, 21]. Recently, we considered the AOV model and investigated [18] how demixing is influenced by the amount of disorder and by its nature. We found that demixing was, to a large extent, only dependent

on the fraction  $f$  of the volume that is not accessible to the colloids due to the presence of the random matrix. The matrix topology was instead largely irrelevant. Moreover, we observed the possibility of capillary condensation of the colloids: for some values of the parameters, a colloid-gas bulk phase is in equilibrium with a colloid-liquid phase in the matrix.

The AOV model completely neglects polymer-polymer interactions, hence it may only be quantitatively predictive close to the  $\theta$  point where, to some extent, polymers behave as ideal particles. In this paper we make a first step towards the inclusion of polymer-polymer interactions, allowing us to study systems under good-solvent conditions. We still use a CG model in which polymers are treated as monoatomic molecules, but we include a polymer-polymer repulsive pair potential which is such to reproduce the correct thermodynamics in the low-density limit. In recent years, this class of CG models has been extensively studied [22–24]. It is now clear that, unless one includes many-body interactions or considers density-dependent potentials, they are quantitatively predictive only in the dilute regime in which the polymer volume fraction  $\eta_p$  [ $\eta_p = c_p/c_p^*$ , where  $c_p = N_p/V$  is the concentration and  $c_p^* = 3/(4\pi R_g^3)$ ] satisfies  $\eta_p \lesssim 1$ . If  $q \lesssim 1$  (the so-called colloid regime), fluid-fluid demixing occurs for  $\eta_p \lesssim 1$ , hence monoatomic CG models are expected to provide reasonably accurate results. If, instead,  $q \gtrsim 1$  (the protein regime), demixing occurs for  $\eta_p \gtrsim 1$ , hence one must use more sophisticated CG multiblob models [25] in which each polymer is represented by a polyatomic molecule and each atom corresponds to a polymer blob of size of the order of that of the colloid. In this paper, we investigate the case  $q = 0.8$ , as in our previous work [18]. Since colloids are larger than polymers, a CG approach based on a single-blob representation of the polymers should be adequate.

The exact polymer-polymer and polymer-colloid pair potentials appropriate for single-blob models have been computed in several papers [4, 24, 26–29]. The polymer-polymer potential has a Gaussian shape with a width of the order of  $R_g$  and is significantly different from zero ( $u_{pp}(r)/u_{pp}(0) \gtrsim 0.01$ ) up to  $r \approx 2.5R_g$ . Analogously, the typical colloid-polymer potential has a tail, which is still significant for  $r \approx 2(R_g + R_c)$ . The presence of these tails makes simulations quite slow, since one must consider a large number of neighboring molecules in each updating step. Since our simulations are extremely complex and time-consuming—we must average over a large number of disorder realizations—we decided to replace the exact potentials with simpler ones that generalize the AOV interactions. They

are square potentials, hence have no tails, and thus allow us to determinate the energy quite fast. Of course, this simplification implies that our results cannot be quantitatively accurate. Still, our simulations should allow us to understand how the presence of the porous matrix changes the behavior of the polymer-colloid mixture under good-solvent conditions.

The paper is organized as follows. In Sec. II we present the simple model which we will use and give the basic definitions. In Sec. III we discuss the model in the bulk, while in Sec. IV we determine the binodal lines and the critical-point positions for polymers and colloids adsorbed in two different colloidal matrices. Finally, in Sec. V we present our conclusions.

## II. DEFINITIONS

### A. Models

In this paper we model polymers as soft effective spheres. Polymers of radius of gyration  $R_g$  are represented by monoatomic molecules interacting with pair potential

$$u_{pp}(r) = \begin{cases} \epsilon_{pp} & \text{for } r < \alpha R_g, \\ 0 & \text{for } r \geq \alpha R_g, \end{cases} \quad (1)$$

where  $\alpha$  and  $\epsilon_{pp}$  are parameters which are fixed below. Since we expect demixing to occur for  $\eta_p \lesssim 1$ , we have fixed  $\alpha$  and  $\epsilon_{pp}$  to reproduce accurately the compressibility factor  $Z = p/(k_B T c)$  ( $p$  is the pressure and  $c$  the concentration) in this density interval. In practice, we have determined the second virial coefficient  $B_{2,pp}$  and  $Z$  at  $\eta_p = 1$  using model (1) for several values of the parameters and we have compared the results with those obtained in full-monomer simulations [30, 31]. Requiring the model to reproduce the estimate [30]  $A_{2,pp} = B_{2,pp} R_g^{-3} \approx 5.50$  and the estimate [31] of  $Z$  for  $\eta_p = 1$ , we obtain

$$\alpha = 1.58 \quad \epsilon_{pp} = 1.096. \quad (2)$$

It is important to note that, although the thermodynamics is quite well reproduced up to  $\eta_p \approx 1$  and with small errors up to  $\eta_p = 2$  (at such value of  $\eta_p$  the difference between  $Z$  computed in the present model and that for polymers is 8%), the intermolecular structure is poorly reproduced. For instance, in this model the intermolecular distribution function is discontinuous and oscillates due to the discontinuity of the potential, a behavior which is not observed in polymer systems.

Let us now introduce the colloids. Two colloids interact with a hard-sphere potential

$$u_{cc}(r) = \begin{cases} \infty & \text{for } r < 2R_c, \\ 0 & \text{for } r \geq 2R_c, \end{cases} \quad (3)$$

while colloid-polymer interactions are modelled by taking a soft version of the AOV hard-core potential

$$u_{cp}(r) = \begin{cases} \epsilon_{cp}(q) & \text{for } r < R_c + R_g, \\ 0 & \text{for } r \geq R_c + R_g. \end{cases} \quad (4)$$

The parameter  $\epsilon_{cp}(q)$  is fixed so that the thermodynamics is exactly reproduced in the low-density limit. For this purpose we compute the universal polymer-colloid second-virial combination

$$\begin{aligned} A_{2,cp} &= B_{2,cp} R_c^{-3/2} R_g^{-3/2} = \frac{1}{2} R_c^{-3/2} R_g^{-3/2} \int d^3\mathbf{r} (1 - e^{-u_{cp}(r)}) = \\ &= \frac{2\pi}{3} (1 - e^{-\epsilon_{cp}}) (1 + q)^3 q^{-3/2}. \end{aligned} \quad (5)$$

Estimates of  $A_{2,cp}$  were obtained in Ref. [29] for polymers under good-solvent conditions. We fix  $\epsilon_{cp}(q)$  so that the value of  $A_{2,cp}$  in our model is the same as that obtained in Ref. [29]. Results are reported in Table I. As expected,  $\epsilon_{cp}(q)$  diverges as  $q \rightarrow 0$ , since in this limit polymers are quite well described by hard spheres. In the opposite limit instead, the interaction energy vanishes, a phenomenon which is related to the fact that, for large values of  $q$ , the polymer can wrap around the hard spheres. Hence, in the CG model in which each polymer is replaced by a monoatomic molecule positioned in the polymer center of mass, there is a significant probability that the CG polymer and the colloid are one on top of the other. If we compare potentials (4) with the exact ones reported in Refs. [27, 29], we observe that  $u_{cp}(r)$ , which is essentially an average potential, overestimates the interaction energy for  $R_g \lesssim r \lesssim R_c + R_g$ , while it significantly underestimates  $u_{cp}(r)$  close to overlap (for instance, the correct  $u_{cp}(r)$  diverges for  $r \rightarrow 0$  if  $q \leq 1$ ). Note that a more accurate model could have been obtained by also introducing a parameter  $\alpha_{cp}$  to specify the range of the polymer-colloid interactions, as in Eq. (1). However, to fix an additional parameter we would have needed some additional thermodynamic information (for instance, the pressure for a finite value of the polymer and colloid densities), which was not available to us.

$q$	$\epsilon_{cp}$
5	0.346
2.5	0.725
1.25	1.363
1	1.642
0.8	2.035

TABLE I: Estimates of the parameter  $\epsilon_{cp}$ .

We mention that a different simplified model including polymer-polymer interactions was introduced in Ref. [32] and studied for  $q = 0.8$ . However, with their parameter choices, thermodynamics is not reproduced in the low-density limit. Indeed, if we consider the second virial coefficients, their model gives  $A_{2,pp} \approx 1.79$  and  $A_{2,cp} \approx 17.2$  to be compared with estimates  $A_{2,pp} \approx 5.50$  and  $A_{2,cp} \approx 14.8$  obtained from direct polymer simulations [29, 30]. While the colloid-polymer coefficient is reasonably close to the correct one (they differ by 15%), the second virial coefficient for polymers is significantly smaller. Hence, the model of Ref. [32] appears to be more appropriate to describe polymers in the crossover region close to the  $\theta$  point than in the good-solvent regime.

The colloidal matrix has been introduced as in our previous work. We consider a random distribution of quenched hard spheres of radius  $R_{\text{dis}}$ . The matrix-colloid and matrix-polymer interaction potentials are therefore:

$$\begin{aligned}
u_{cd}(r) &= \begin{cases} \infty & \text{for } r < R_{\text{dis}} + R_c, \\ 0 & \text{for } r \geq R_{\text{dis}} + R_c, \end{cases} \\
u_{pd}(r) &= \begin{cases} \epsilon_{cp}(q_{\text{dis}}) & \text{for } r < R_{\text{dis}} + R_g, \\ 0 & \text{for } r \geq R_{\text{dis}} + R_g, \end{cases} \tag{6}
\end{aligned}$$

where  $q_{\text{dis}} \equiv R_g/R_{\text{dis}}$ . For  $R_{\text{dis}} \rightarrow 0$ , i.e., for  $q_{\text{dis}} \rightarrow \infty$ , we have  $\epsilon_{cp}(q_{\text{dis}}) \rightarrow 0$ . As we already discussed, this reflects the fact that the polymer can easily wrap around the small quenched colloid, which implies that the CG polymer can easily overlap with it. As a consequence of this, the matrix becomes less and less repulsive as  $q_{\text{dis}}$  increases, so that in the limit  $R_{\text{dis}} \rightarrow 0$ , i.e.  $q_{\text{dis}} \rightarrow \infty$ , we obtain bulk behavior. This is, of course, an artifact of the model, which

can only be eliminated by using multiblob approaches [25], in which a single polymer is represented by many blobs, whose size is of the order of that of the quenched colloid.

In the simple model we consider, disorder is characterized by two parameters, the reduced concentration  $\hat{c} \equiv c_{\text{dis}} R_c^3$  ( $c_{\text{dis}} = N_{\text{dis}}/V$ , where  $N_{\text{dis}}$  is the number of quenched hard spheres present in the volume  $V$ ) and the ratio  $R_{\text{dis}}/R_c$ . However, as we already discussed in Ref. [18], it is much more useful to characterize the amount of disorder by using the volume fraction  $f$  which is not accessible to the colloids due to the matrix. To define it precisely, consider the region  $\mathcal{R}$  in which the (centers of the) colloids are allowed:

$$\mathcal{R} = \{ \mathbf{r} : |\mathbf{r} - \mathbf{r}_i| \geq R_c + R_{\text{dis}}, \text{ for all } 1 \leq i \leq N_{\text{dis}} \}, \quad (7)$$

where  $\mathbf{r}_i$  is the position of the  $i$ -th hard sphere belonging to the matrix. If  $V_{\mathcal{R}}$  is the volume of the region  $\mathcal{R}$ , we define

$$f \equiv 1 - \frac{[V_{\mathcal{R}}]}{V}, \quad (8)$$

where  $[V_{\mathcal{R}}]$  is the average of  $V_{\mathcal{R}}$  over the different matrix realizations.

## B. Simulation details

In this work we investigate the effect of disorder on the fluid-fluid binodals for  $q = 0.8$  which is the case we investigated in our previous work [18]. We perform simulations in the absence of the porous matrix and for  $f = 0.4$ ,  $R_{\text{dis}}/R_c = 0.2, 1.0$ . In order to determine the coexistence curves we combine the grand-canonical algorithm with the umbrella sampling [33] and the simulated-tempering method [34], as discussed in the Appendix of Ref. [18].

The grand partition sum for each disorder realization is

$$\Xi(V, z_p, z_c) = \sum_{N_p, N_c} z_p^{N_p} z_c^{N_c} Q(V, N_p, N_c), \quad (9)$$

where  $Q(V, N_p, N_c)$  is the configurational partition function of a system of  $N_p$  polymers and  $N_c$  colloids in a volume  $V$ , and  $z_p$  and  $z_c$  are the corresponding fugacities. In Eq. (9) we normalize  $Q(V, N_p, N_c)$  so that  $Q(V, 1, 0) = Q(V, 0, 1) = V$ , hence  $z_p$  and  $z_c$  are dimensionful parameters.

The system shows, both in the bulk and in the matrix, a demixing transition. For  $z_p < z_{p,\text{crit}}$  a single phase exists, while for  $z_p > z_{p,\text{crit}}$  coexistence is observed along the line  $z_c =$



$z_c^*(z_p)$ . In the MC simulations the position of the demixing curve can be determined by studying the disorder averaged histograms of  $N_c$  and  $N_p$ , which are defined as

$$\begin{aligned} h_{c,\text{ave}}(N_{c,0}, z_p, z_c) &\equiv \left[ \langle \delta(N_c, N_{c,0}) \rangle_{GC, z_p, z_c} \right], \\ h_{p,\text{ave}}(N_{p,0}, z_p, z_c) &\equiv \left[ \langle \delta(N_p, N_{p,0}) \rangle_{GC, z_p, z_c} \right], \end{aligned} \quad (10)$$

where  $\delta(x, y)$  is Kronecker's delta [ $\delta(x, x) = 1$ ,  $\delta(x, y) = 0$  for  $x \neq y$ ],  $\langle \cdot \rangle_{GC, z_p, z_c}$  is the grand-canonical ensemble average, and  $[\cdot]$  is the average over the matrix realizations. In the two-phase region the histograms show a double-peak structure. In order to obtain  $z_c^*$  at fixed  $z_p$  in a finite volume, several different methods can be used. We followed two different recipes, the equal-area and the equal-height methods, as discussed in Ref. [18]. They give completely consistent results: the results we report have been obtained by using the equal-height method.

### III. BULK BEHAVIOR

Before considering the model in the presence of the matrix, we determine the phase behavior in the bulk. We use the algorithm described in Ref. [18]. One Monte Carlo iteration consists in 3 simulated-tempering fugacity swaps and 1000-5000 grand-canonical moves in which colloids and polymers are inserted or removed. For each value of  $z_p$ , we perform  $N_{\text{ini}}$  iterations to determine the umbrella functions and then  $N_{\text{iter}}$  iterations to measure the histograms. Typically,  $N_{\text{ini}}$  varies between  $5000 N_m$  and  $20000 N_m$ , while  $N_{\text{iter}}$  is of the order of  $5 \cdot 10^6 N_m$ . Here  $N_m$  is the number of colloid fugacities which are sampled together in the simulated-tempering simulation; we take  $N_m \approx 10$ .

The demixing curves have been determined for  $L/R_c = 14$  and  $L/R_c = 16$ , to identify size effects. We have also performed simulations for  $L/R_c = 13$  close to the critical point, to better determine its position. In Fig. 1 we report the liquid-gas coexistence curve in terms of the colloid and polymer volume fractions  $\eta_c$  and  $\eta_p$  defined as

$$\eta_c = \frac{4}{3} \pi c_c R_c^3, \quad \eta_p = \frac{4}{3} \pi c_p R_g^3, \quad (11)$$

where  $c_c$  and  $c_p$  are the concentrations of the colloids and of the polymers, respectively. It is clear that size effects are quite small, indicating that our results provide a good estimate of the true (infinite-volume) binodal curve. As already observed in Ref. [4], the presence

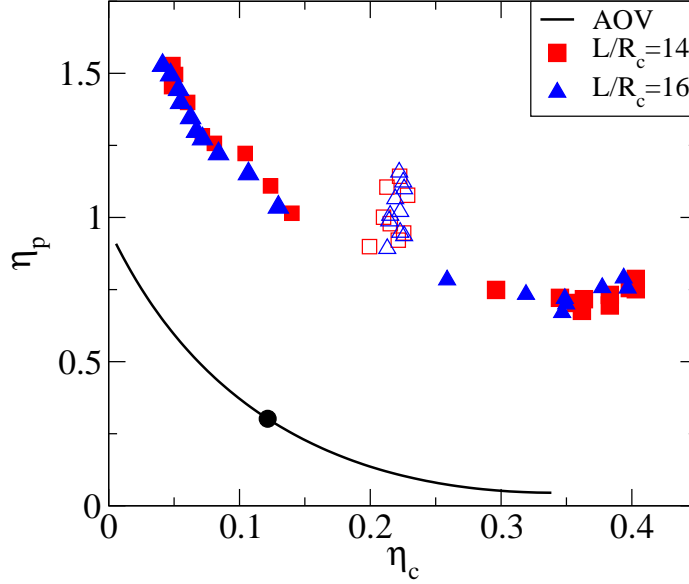


FIG. 1: (Color online) Bulk demixing curve (solid symbols) and coexistence diameter (empty symbols) in the  $(\eta_c, \eta_p)$  system representation for  $L/R_c = 14, 16$ . We also report the demixing curve of the AOV model, solid line, from Ref. [18]; the solid circle gives the position of the critical point.

of polymer-polymer interactions significantly changes the binodal curve: the values of  $\eta_p$  at which demixing occurs are significantly larger in the presence of polymer interactions than in the AOV case. An unusual feature of our results for the coexistence curve is that  $\eta_p$  along the coexistence line in the colloid-liquid phase slightly increases as  $\eta_c$  increases beyond 0.35. This feature is not observed in the more accurate model used in Ref. [4], nor in experiments. It is probably an artifact of the model, a consequence of the discontinuous nature of the potentials or of the fact that polymers and colloids can overlap paying a relatively small energy penalty of the order of  $2k_B T$ , a phenomenon which is not possible in the exact representation.

We also report the liquid-gas demixing curve in the reservoir representation. We report the results in terms of the (ideal) reservoir packing fraction

$$\eta_p^{r,\text{id}} \equiv \frac{4\pi}{3} z_p R_g^3, \quad (12)$$

which is the quantity used in the AOV model, and in terms of the reservoir packing fraction

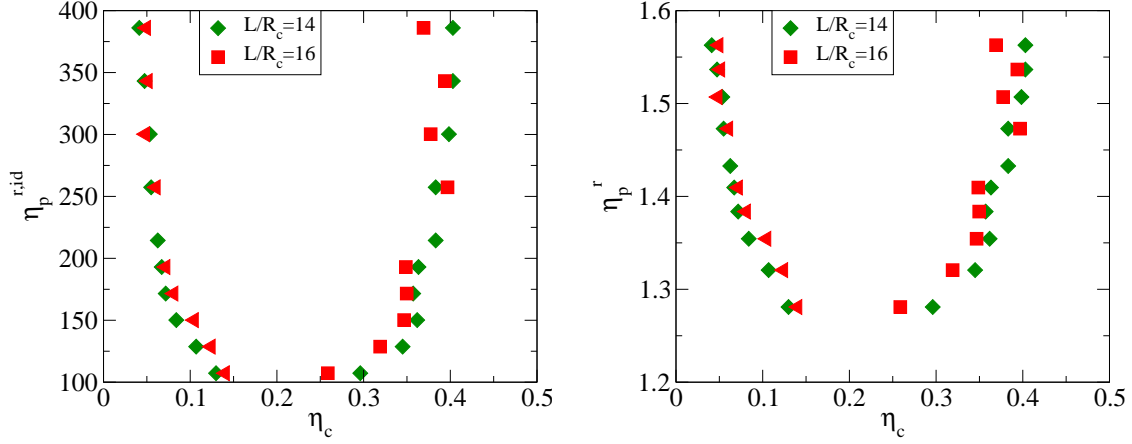


FIG. 2: (Color online) Bulk demixing curve in the reservoir representation for  $L/R_c = 14, 16$ .  $\eta_p^{r,id}$  is the ideal reservoir packing fraction, while  $\eta_p^r$  is the true reservoir packing fraction.

$\eta_p^r$ , which is the volume fraction of the polymers in the absence of colloids at a given  $z_p$ . We have determined it by grand-canonical simulations setting  $z_c = 0$ . The two quantities  $\eta_p^{r,id}$  and  $\eta_p^r$  are related by

$$\eta_p^{r,id} = \eta_p^r \exp[\beta \mu_p^{(exc)}(\eta_p^r)], \quad (13)$$

where  $\mu_p^{(exc)}(\eta_p^r)$  is the polymer excess chemical potential which can be computed by using the equation of state. In Fig. 2 we report the liquid-gas coexistence curve by using both definitions. Size effects are small also in this case, except close to the critical point. It is interesting to compare the binodal curve in the  $(\eta_c, \eta_p^r)$  plane with that of the AOV model presented in Ref. [11] (see their Fig. 3). The curve here is significantly more symmetric and shifted towards larger values of  $\eta_p^r$ .

Finally, we determine the critical point by using the standard cumulant method (we essentially follow Ref. [32]). The order parameter associated with the critical transition can be identified as [32]

$$m \equiv \eta_c - \langle \eta_c \rangle, \quad (14)$$

where  $\langle \eta_c \rangle$  is the average colloid volume fraction. Then, we consider the Binder cumulants at coexistence

$$M(z_p, L) \equiv \frac{\langle m^2 \rangle}{\langle |m| \rangle^2} \Big|_{z_c = z_c^*(z_p)} \quad U(z_p, L) \equiv \frac{\langle m^4 \rangle}{\langle m^2 \rangle^2} \Big|_{z_c = z_c^*(z_p)}. \quad (15)$$

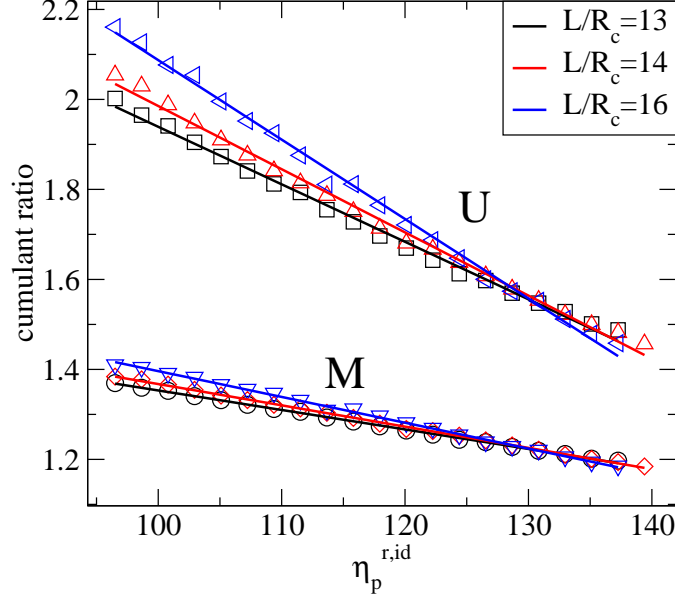


FIG. 3: (Color online) Cumulant ratios  $M$  and  $U$  at coexistence as a function of  $\eta_p^{r,\text{id}}$  for several values of  $L/R_c$ .

The cumulants for different values of  $L$  are reported in Fig. 3 as a function of  $\eta_p^{r,\text{id}}$  for three different values of  $L/R_c$ . The critical point is given by the intersection point. Both cumulants have approximately the same intersection point, which allows us to estimate

$$\eta_{p,\text{crit}}^{r,\text{id}} = 129(2), \quad \eta_{p,\text{crit}}^r = 1.321(4). \quad (16)$$

At the intersection  $M$  and  $U$  assume the values

$$M_{\text{crit}} = 1.226(5), \quad U_{\text{crit}} = 1.57(2), \quad (17)$$

which are close to those appropriate for the Ising three-dimensional universality class:  $M_{\text{crit}} \approx 1.239$  [35] and  $U_{\text{crit}} = 1.6036(1)$  [36]. The small differences we observe are due to field-mixing effects [37, 38], which we have not taken into account in the present analysis. At the critical point we obtain

$$\eta_{c,\text{crit}} = \langle \eta_c \rangle = 0.22(1), \quad \eta_{p,\text{crit}} = \langle \eta_p \rangle = 0.93(2). \quad (18)$$

Note that these estimates are very different from those of the AOV critical point [11, 12]:

$$\eta_{c,\text{crit}} = 0.1340(2), \quad \eta_{p,\text{crit}} = 0.3562(6). \quad (19)$$

		$q$	$\eta_{c,\text{crit}}$	$\eta_{p,\text{crit}}$
Expt.	Ref. [39]	0.49	0.21(1)	1.00(5)
Expt.	Ref. [40]	0.57	0.2	0.6
Expt.	Ref. [41]	0.86	0.11	0.5
Expt.	Ref. [42]	0.92	0.195	1.21
Expt.	Ref. [43]	1.00	0.2	0.5
MC	Ref. [4]	0.34	0.20	0.29
		0.67	0.19	0.40
		1.05	0.18	0.51
This work		0.80	0.22(1)	0.93(2)

TABLE II: Experimental (Expt) and Monte Carlo (MC) estimates [44] of  $\eta_{c,\text{crit}}$  and  $\eta_{p,\text{crit}}$ . An extensive list of results can be found in Sec. 8 of Ref. [45].

Both the colloid and the polymer critical volume fractions increase quite significantly.

The estimate (18) of the colloid critical volume fraction agrees with all experimental and theoretical estimates, see Table II for a list of results. On the other hand, the estimate of the polymer volume fraction is not consistent with the results of Bolhuis *et al.* [4], which used a much more accurate description of the pair interactions. The discrepancy is probably due to our choice of simplified interactions and, in particular, to the fact that polymers and colloids can overlap with a relatively small energy penalty. Clearly, quantitative predictions require a much more accurate modelling of the interactions among polymers and colloids. We also report some experimental results which show, however, large discrepancies. They are of little use for quantitative comparisons. We finally mention the results of Ref. [32]:  $\eta_{p,\text{crit}}^{r,\text{id}} = 1.282(2)$ ,  $\eta_{c,\text{crit}} = 0.150(2)$ , and  $\eta_{p,\text{crit}} = 0.328(2)$ . As we already discussed, this model is more appropriate for polymers close to the  $\theta$  point and, indeed, the estimates of the volume fractions at criticality are close to the AOV ones.

The critical point can also be approximately determined from the behavior of the coexistence diameter given by

$$(\eta_{c,\text{diam}}, \eta_{p,\text{diam}}) \equiv \left( \frac{\eta_{c,\text{liq}} + \eta_{c,\text{gas}}}{2}, \frac{\eta_{p,\text{liq}} + \eta_{p,\text{gas}}}{2} \right). \quad (20)$$

If we consider the intersection of the diameter with a simple interpolation of the coexistence

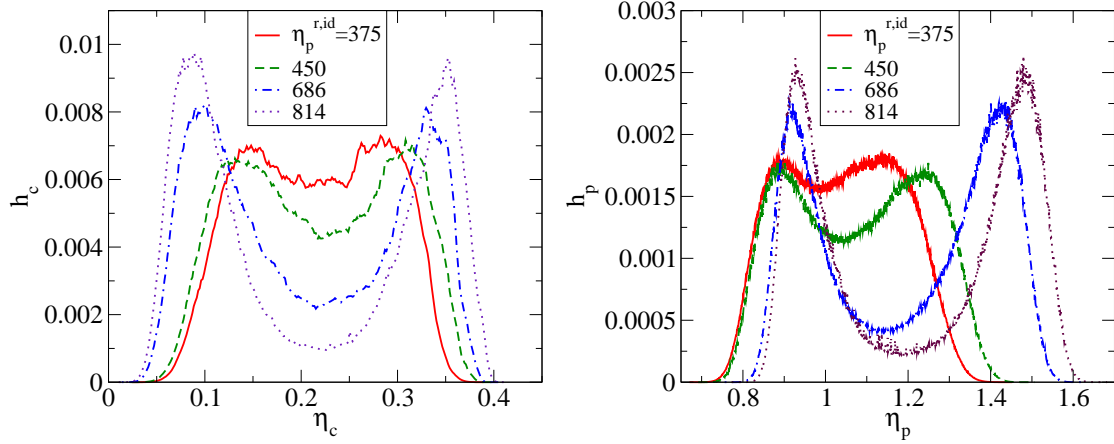


FIG. 4: (Color online) Colloid (left) and polymer (right) volume fraction histograms at coexistence for several values of  $\eta_p^{r,id}$ , for  $(f, R_{\text{dis}}/R_c) = (0.4, 1.0)$ ,  $L/R_c = 14$ .

data, we obtain  $\eta_{c,\text{crit}} \simeq 0.21$  and  $\eta_{p,\text{crit}} \simeq 0.89$ . The critical colloid fugacity is consistent with estimate (18), while the critical polymer fugacity is only slightly underestimated. Size corrections, which are not taken into account in this simpler approach, are apparently small in the bulk, even at the critical point. As we shall see in the next section, this is no longer the case in the presence of the matrix.

#### IV. DEMIXING IN THE PRESENCE OF A POROUS MATRIX

We now study the demixing in the presence of the matrix for a mixture with  $q = 0.8$ . We take disorder parameters analogous to those used in our previous work [18]: we consider  $f = 0.4$  and two different sizes of the quenched colloids,  $R_{\text{dis}}/R_c = 0.2$  and  $1.0$ . Correspondingly,  $c_{\text{dis}}R_c^3 = 0.070, 0.014$  in the two cases, respectively. To determine size effects we simulate systems with  $L/R_c = 12, 14, 16$ . We use the same algorithm used in the bulk [18], setting  $N_{\text{iter}}$ , the number of iterations during which histograms are measured, equal to  $40000N_m$ . Each histogram is averaged over 400 different matrix realizations. Note that system sizes are smaller than those used in the AOV case. This is due to the fact that here we are dealing with larger polymer volume fractions, hence simulations of the interacting model are significantly more time-consuming than AOV simulations of systems of the same size. This significantly limits the size of the systems we can simulate.

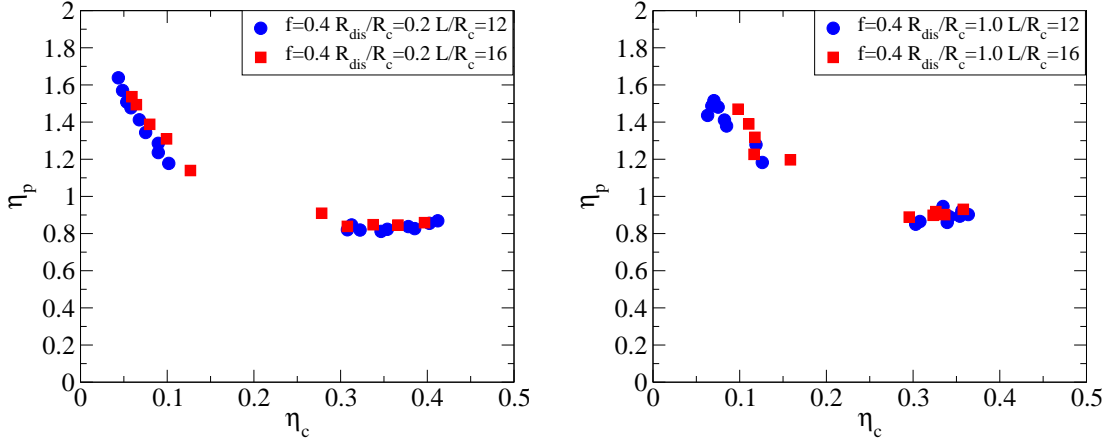


FIG. 5: (Color online) Fluid-fluid binodal curves for  $f = 0.4$ ,  $R_{\text{dis}}/R_c = 0.2$  (left),  $f = 0.4$ ,  $R_{\text{dis}}/R_c = 1.0$  (right). We report the results for  $L/R_c = 12$  and  $L/R_c = 16$  in terms of  $\eta_c$  and  $\eta_p$ .

### A. Demixing curves

In order to determine the coexistence line  $z_c = z_c^*(z_p)$  in the  $(z_c, z_p)$  plane, we analyze the colloid and polymer averaged histograms defined in Eq. (10) using the equal-height method (completely equivalent results are obtained using the equal-area method, see Ref. [18]): coexistence is defined as the value of  $z_c$  such that the colloid (or polymer) histogram has two peaks of equal height. The histograms at coexistence for  $R_{\text{dis}}/R_c = 1$  are shown in Fig. 4 for  $L/R_c = 14$  and several values of  $\eta_p^{r,\text{id}}$ . As expected, as  $\eta_p^{r,\text{id}}$  increases, the two peaks become more pronounced,  $\eta_{c,\text{gas}}$  (the colloid volume fraction in the colloid-gas phase) decreases, while  $\eta_{c,\text{liq}}$  (the same quantity in the colloid-liquid phase) increases. As in the bulk case, the behavior of the polymer histograms is more peculiar, since the polymer volume fraction apparently increases in both phases, except close to the critical point. Again, we expect this to be an artifact of the model, due to the simplifications we have introduced. It is interesting to stress a second difference with respect to the AOV case. While the AOV histograms are strongly asymmetric, with a broad colloid-gas peak and a narrow colloid-liquid peak, in the presence of interactions the two peaks are much more symmetric. As a consequence, the different methods we used to determine coexistence, the equal-height and the equal-area methods (see Ref. [18] for the precise definitions) give fully consistent results, both for the colloid and polymer densities at coexistence and for the value  $z_c^*$ , for all values of  $L$ .

In Fig. 5 we report our results for the demixing curves in terms of  $\eta_c$  and  $\eta_p$  for two

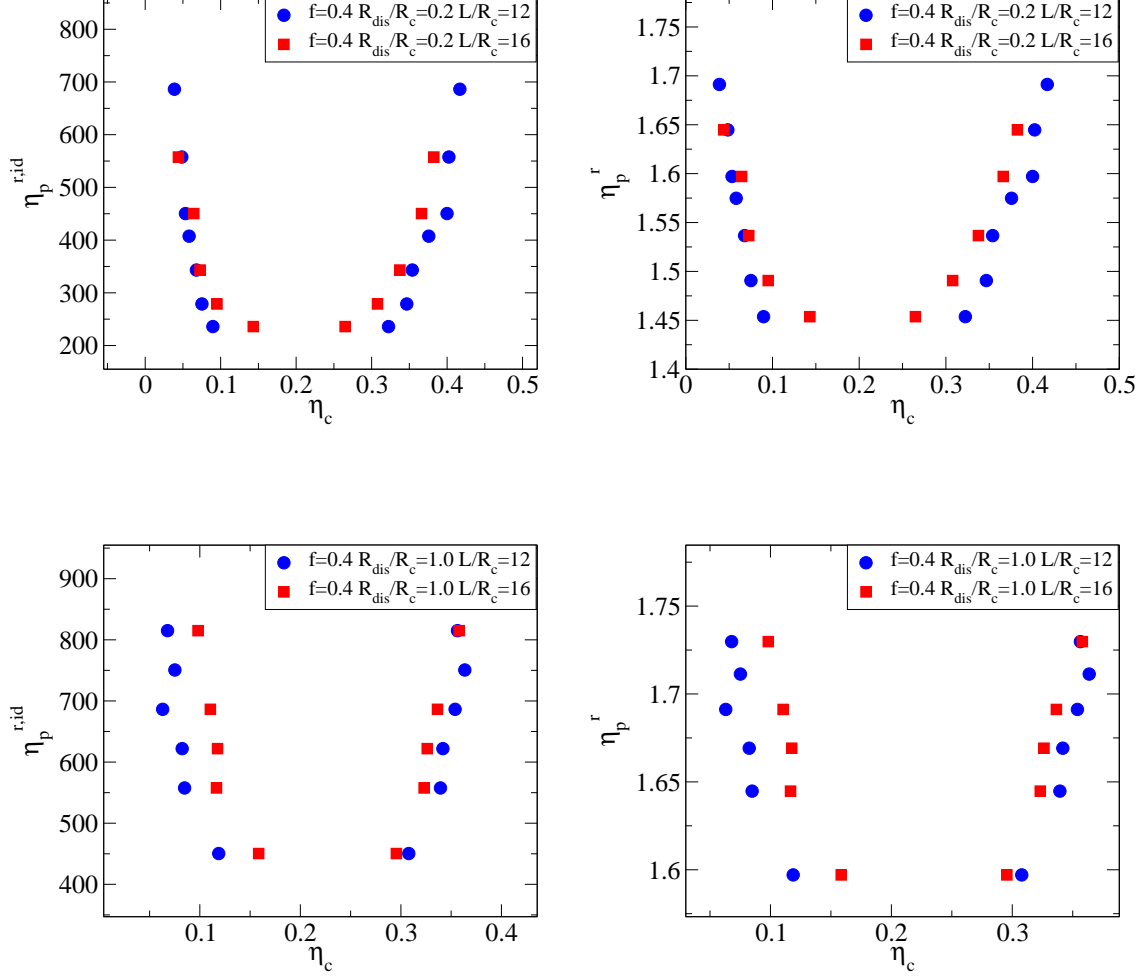


FIG. 6: (Color online) Fluid-fluid binodal curves for  $f = 0.4$ ,  $R_{\text{dis}}/R_c = 0.2$  (top) and  $f = 0.4$ ,  $R_{\text{dis}}/R_c = 1.0$  (bottom). We report the results for  $L/R_c = 12$  and  $L/R_c = 16$  in terms of  $\eta_c, \eta_p^{r,\text{id}}$  (left) and  $\eta_c, \eta_p^r$  (right).

values of  $L/R_c$ . For  $R_{\text{dis}}/R_c = 0.2$  size corrections are small and thus our data allow us to determine reliably the infinite-volume coexistence curve. For  $R_{\text{dis}}/R_c = 1$  we observe instead some size effects on the colloid-gas branch of the binodal: at a given  $\eta_c$ , the value of  $\eta_p$  along the binodal increases as  $L/R_c$  is increased from 12 to 16. On the scale of the figure, the change is small: quantitatively it amounts to an increase of the order of 5-10%. In Fig. 6 we show the fluid binodals in the reservoir representation, using both  $\eta_p^{r,\text{id}}$  and  $\eta_p^r$ , as we did in the bulk case. For  $R_{\text{dis}}/R_c = 0.2$  size corrections appear to be under control, except close to the critical point. For  $R_{\text{dis}}/R_c = 1$  corrections are instead larger, especially



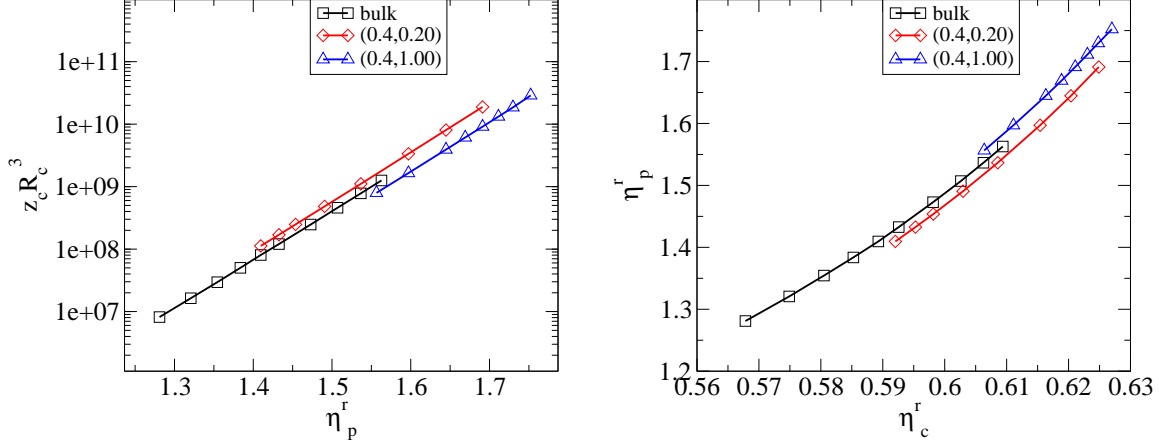


FIG. 7: (Color online) Estimates of  $z_c^* R_c^3$  as a function of the reservoir polymer volume fraction  $\eta_p^r$  (left) and of  $\eta_p^{r*}$  at coexistence in terms of the reservoir colloid volume fraction  $\eta_c^r$  (right). Results for  $L/R_c = 14$ .

for the colloid-gas branch, which cannot be reliably determined even far from the critical point, where size corrections should be smaller. Clearly, accurate estimates require much larger values of  $L/R_c$ .

In Fig. 7 we report  $z_c^* R_c^3$  at coexistence as a function of  $\eta_p^r$  and also  $\eta_p^{r*}$  at coexistence in terms of the reservoir colloid volume fraction  $\eta_c^r$ , which represents the volume fraction at the given value of  $z_c$ , in the absence of polymers and matrix [46]. Note that, on a logarithmic scale, the quantity  $z_c^* R_c^3$  lies quite precisely on a straight line, indicating that the colloid chemical potential at coexistence is well approximated by a linear function in  $\eta_p^r$ . This feature was already observed in the AOV case and seems to be a general feature of this type of systems. Fig. 7 differs significantly from that obtained in the AOV case. There, the binodal curves showed a significant dependence on  $f$ , while here the bulk curve approximately falls on top of those corresponding to  $f = 0.4$ : they only differ for the position of the critical point. This implies that a colloid-liquid bulk phase is almost always in equilibrium with a colloid-liquid phase in the matrix, and so does a colloid-gas phase: no capillary condensation or evaporation is observed except in a very tiny parameter range, i.e. for those  $(\eta_c^r, \eta_p^r)$  that belong to the tiny region between the bulk and matrix binodal curve.

## B. Critical point

We wish now to estimate the position of the critical points. This is not an easy task in these systems, since the transition belongs to the universality class of the random-field Ising model (RFIM) [14–17]. Size corrections are large and the efficient cumulant method we used for the bulk case does not work. Therefore, we must adopt a different strategy: we follow closely Ref. [15]. First, for each matrix realization we define the averages  $\langle N_c^k \rangle_{\text{vap}}$  and  $\langle N_c^k \rangle_{\text{liq}}$  in the vapor and liquid phases. They are defined as

$$\begin{aligned}\langle N_c^k \rangle_{\text{vap}} &= \frac{1}{K_{\text{vap}}} \int \theta(N_{c,\text{int}} - N_c) P(N_c) N_c^k, \\ \langle N_c^k \rangle_{\text{liq}} &= \frac{1}{K_{\text{liq}}} \int \theta(N_c - N_{c,\text{int}}) P(N_c) N_c^k.\end{aligned}\tag{21}$$

Here  $P(N_c)$  is the histogram of  $N_c$  at coexistence for the given matrix realization,  $N_{c,\text{int}}$  gives the position of the minimum between the two peaks,  $\theta(x)$  is Heaviside step function [ $\theta(x) = 1$  for  $x > 0$  and  $\theta(x) = 0$  for  $x < 0$ ], and  $K_{\text{vap}}$  and  $K_{\text{liq}}$  are normalization factors. Then, for each phase, we define the connected susceptibility [15]

$$\chi = \frac{[\langle N_c^2 \rangle - \langle N_c \rangle^2]}{V},\tag{22}$$

where  $[\cdot]$  is the average over disorder and  $V$  is the volume of the box. Essentially,  $\chi_{\text{vap}}$  and  $\chi_{\text{liq}}$  measure the average squared width of the liquid and vapor peaks for each given sample.

In Fig. 8 we report the connected susceptibilities for  $f = 0.4$ ,  $R_{\text{dis}}/R_c = 0.2, 1$  and  $L/R_c = 12, 14, 16$ . While the results for  $R_{\text{dis}}/R_c = 0.2$  are reasonably smooth, the data for  $R_{\text{dis}}/R_c = 1$  are scattered with quite large error bars (we do not even report the data at  $L/R_c = 16$ , since they would make the figure unreadable). This is probably due to the small number of samples we are using. Indeed, in Ref. [15] it was shown that sample-to-sample fluctuations may be quite large and require a particularly large number of different matrix realizations to be controlled. In their case, they averaged over 2000-3000 different realizations, a number which is significantly larger than ours: we only have 400 different samples. In spite of the large errors, the data are, at least qualitatively, in agreement with the expected behavior:  $\chi(L, \eta_p^r)$  increases with  $L$  at fixed  $\eta_p^r$ , while, at fixed  $L$ , it first increases and then decreases as a function of  $\eta_p^r$ , as also observed in Ref. [15].

General renormalization-group arguments indicate that, close to the critical point, the

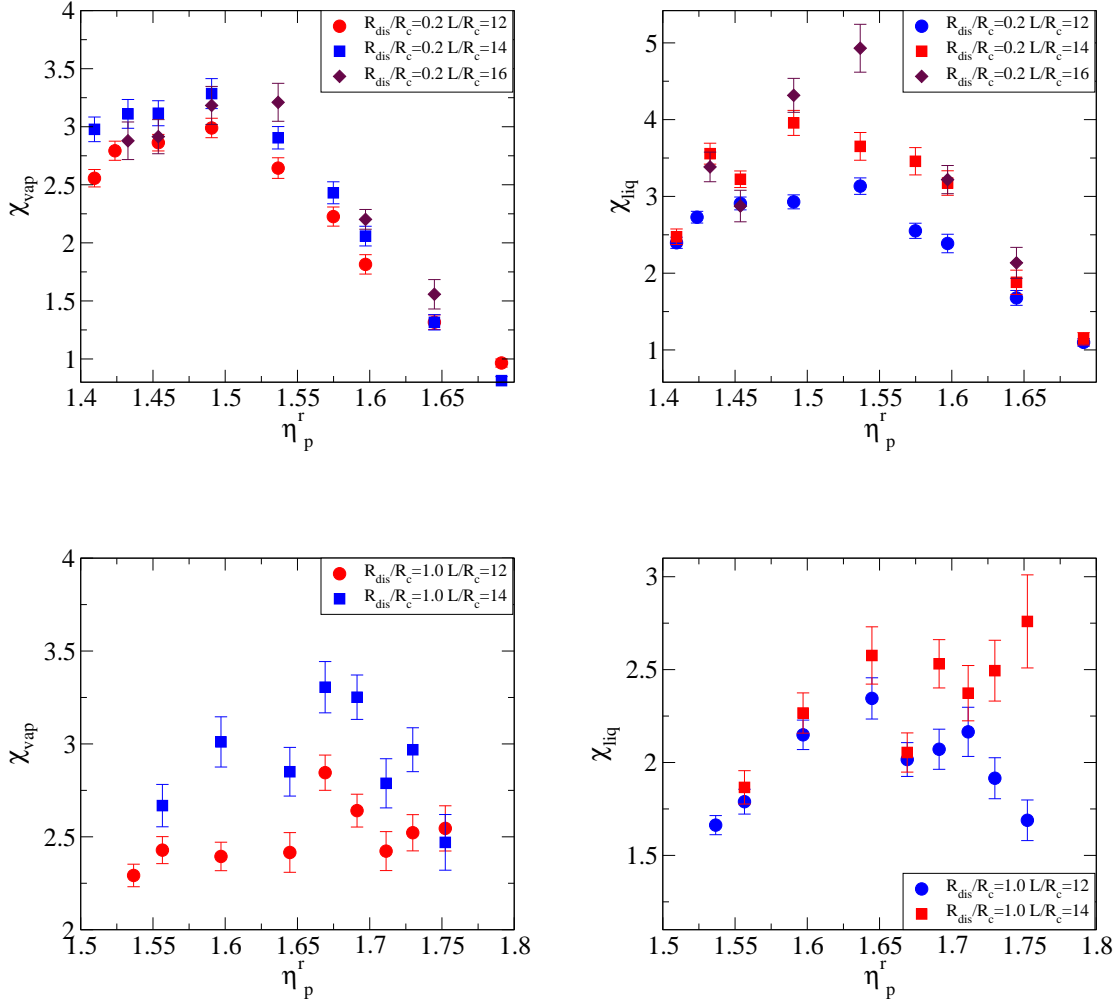


FIG. 8: (Color online) Connected susceptibilities  $\chi$  in the colloid-vapor (left) and in the colloid-liquid (right) phases for  $f = 0.4$ ,  $R_{\text{dis}}/R_c = 0.2$  (top) and  $R_{\text{dis}}/R_c = 1$  (bottom). We report the results for  $L/R_c = 12, 14, 16$  as a function of  $\eta_p^r$ .

susceptibility satisfies the finite-size scaling Ansatz

$$\chi = (L/R_c)^{\gamma/\nu} F[t(L/R_c)^{1/\nu}], \quad (23)$$

where  $\gamma$  and  $\nu$  are critical exponents,  $F(x)$  is a scaling function, and  $t \equiv \eta_p^r/\eta_{p,\text{crit}}^r - 1$  measures the “distance” from the critical point. This scaling Ansatz is, strictly speaking, valid in the limit  $L \rightarrow \infty$ ,  $t \rightarrow 0$  at fixed  $t(L/R_c)^{1/\nu}$  and neglects (analytic and nonanalytic) scaling corrections.

As discussed at length in Refs. [14–17, 19], the critical transition belongs to the RFIM

	$\nu$	$\eta$
Newman & Barkema [47]	1.02(6)	0.15(7)
Hartmann & Young [48]	1.32(7)	0.50(3)
Middleton & Fisher [49]	1.37(9)	0.51(3)
Vink <i>et al.</i> [15]	1.1	0.13
Fernandez <i>et al.</i> [50]	0.90(15)	0.531(40)

TABLE III: Estimates of the critical exponents  $\nu$  and  $\eta$  for the RFIM universality class. The exponent  $\gamma$  is related to  $\nu$  and  $\eta$  by  $\gamma/\nu = 2 - \eta$ .

universality class. Some numerical estimates of the RFIM critical exponents are reported in Table III. It is evident that there is no general consensus on the estimates and thus we tried all different possibilities. Let us first consider the data for  $R_{\text{dis}}/R_c = 0.2$ , which are the most precise. We determine the critical polymer fugacity  $z_{p,\text{crit}}$ , or equivalently  $\eta_{p,\text{crit}}^r$ , by requiring the estimates of  $\chi L^{-\gamma/\nu}$  to collapse onto a single curve as a function of  $tL^{1/\nu}$ , fixing the exponents to the RFIM values. If we use the numerical values of the exponents employed in Ref. [15], we obtain a poor collapse of the data for any choice of the critical polymer fugacity. Apparently, the best collapse is obtained by taking the latest numerical estimates of Ref. [50]. The rescaled data are reported in Fig. 9 and allow us to estimate the scaling function  $F(x)$  appearing in the scaling Ansatz (23). This function is universal apart from two rescalings: if  $F_1(x)$  and  $F_2(x)$  are determined for two different transitions belonging to the same universality class, then one should have  $F_1(x) = aF_2(bx)$ , for suitable, nonuniversal constants  $a$  and  $b$ . We can thus compare the curves appearing in Fig. 9 with the analogous ones reported in Ref. [15]. Shapes are quite similar, although in our case the peak of the scaling functions apparently occurs for  $x \approx 0$ , while in Ref. [15] the maximum occurs for  $x$  well below zero. The origin of this difference is unclear: it might be due to the different choices for the RFIM critical exponents or to the neglected scaling corrections. The results for the critical parameters are reported in Table IV. It is interesting to compare these results with those which would be obtained by a more naive analysis of the diameters. If we compute the intersection of the diameter line with an interpolation of the binodal data for  $L/R_c = 14$  we would obtain  $\eta_{p,\text{crit}} = 1.02$ ,  $\eta_{c,\text{crit}} = 0.20$ . The critical colloid volume

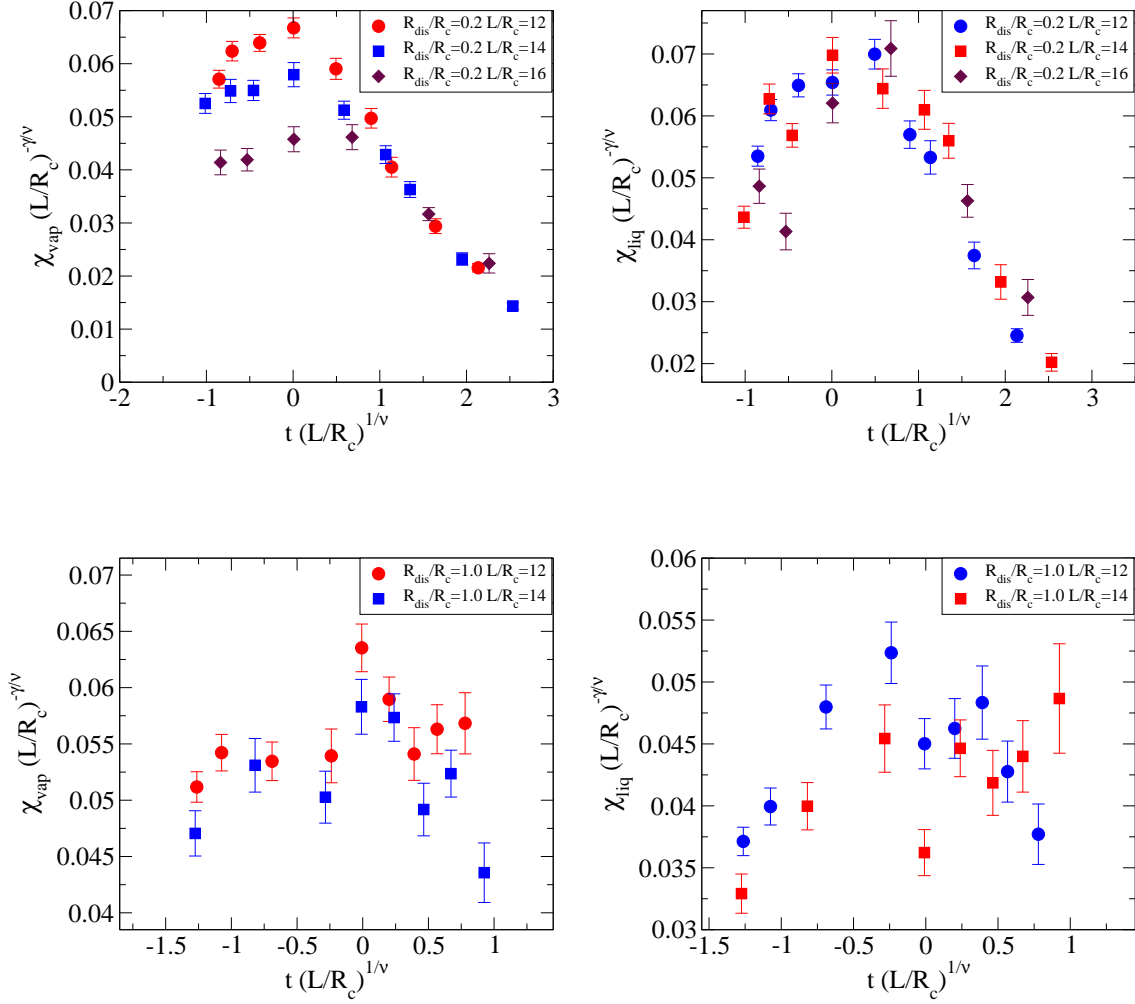


FIG. 9: (Color online) Rescaled connected susceptibilities  $(L/R_c)^{-\gamma/\nu}\chi$  as a function of  $t(L/R_c)^{1/\nu}$ , where  $t \equiv \eta_p^r/\eta_{p,\text{crit}}^r - 1$ , for  $L/R_c = 12, 14, 16$ . Data for  $f = 0.4$ ,  $R_{\text{dis}}/R_c = 0.2$  (top) and  $R_{\text{dis}}/R_c = 1$  (bottom). We use [50]  $\gamma/\nu = 1.5$ ,  $\nu = 0.9$ .

fraction agrees within errors with that reported in Table IV, while  $\eta_{p,\text{crit}}$  is slightly (6%) underestimated.

It is not easy to extend the analysis to the case  $R_{\text{dis}}/R_c = 1$ , given the very large fluctuations in the data. A reasonable collapse, see Fig. 9, is obtained for the parameter choices given in Table IV. However, errors cannot be reliably estimated. Note that size corrections are quite significant for this size of the quenched colloids. For instance, half of the points for which we observe bimodal histograms belong to the homogeneous phase in the infinite-volume limit (compare the estimate of  $\eta_{p,\text{crit}}^r$  with the data reported in the right-bottom panel

$f$	$R_{\text{dis}}/R_c$	$\eta_{p,\text{crit}}^r$	$\eta_{c,\text{crit}}^r$	$\eta_{p,\text{crit}}$	$\eta_{c,\text{crit}}$
bulk		1.321(4)	0.575(1)	0.93(2)	0.22(1)
0.4	0.2	1.49(6)	0.602(4)	1.08(2)	0.21(1)
	1.0	1.67	0.62	1.17	0.22

TABLE IV: Estimates of the critical point position.

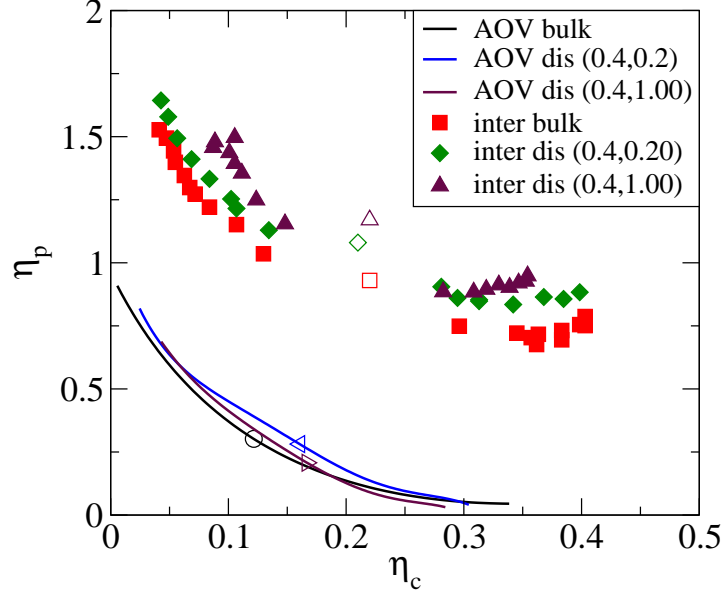


FIG. 10: (Color online) Binodal curves for the interacting-polymer model (solid symbols) and for the AOV model (lines). Empty symbols give the critical points.

of Fig. 6).

## V. CONCLUSIONS

In this paper we consider a simplified CG model for polymer-colloid mixtures. Polymers are represented by point particles interacting by means of pair potentials. Models of this type have been shown to be quantitatively predictive as long as the polymer density is below the overlap density, i.e. for  $\eta_p \lesssim 1$ . Hence, they can be used in the study of mixtures in the colloid regime ( $q \lesssim 1$ ), in which fluid-fluid phase separation occurs for  $\eta_p \lesssim 1$ . We study

polymer-colloid segregation in the bulk and in the presence of a porous matrix for  $f = 0.4$  and for two different values of  $R_{\text{dis}}/R_c$ , 0.2 and 1. In Fig. 10 we summarize our results for the coexistence curves and compare them with the AOV ones. The effect of the matrix is similar in the AOV and in the present interacting model. Disorder moves—but the effect is not large—the coexistence curve towards larger polymer densities. In the colloid-gas phase (for  $\eta_c = 0.1$ , say), the observed change is quantitatively similar in the two models. The volume fraction  $\eta_p^*$  at coexistence increases by 10-20% both in the interacting and in the AOV case as  $f$  increases from  $f = 0$  (bulk) to  $f = 0.4$ . The behavior in the colloid-liquid phase is instead quantitatively slightly different. In the AOV case, the  $f$ -dependence of the coexistence curve is very small (all curves coincide within errors), while in the interacting case the behavior is analogous to that observed in the colloid-gas phase:  $\eta_p^*$  at coexistence increases by 10-20%. It is important to stress that this different behavior may be an artifact of the model, since, as we have already observed several times, binodals cannot be trusted for  $\eta_c \gtrsim 0.35$ .

While binodals do not change significantly with disorder in both cases, the critical point position changes significantly. Moreover, the behavior is quite different in the AOV and in the interacting-polymer model. In the AOV case the critical colloid volume fraction increases significantly as  $f$  changes from zero (bulk case) to 0.4 and 0.7, while  $\eta_{p,\text{crit}}$  is approximately constant or slightly decreases: for  $f = 0$ ,  $\eta_{c,\text{crit}} = 0.1340(2)$  and  $\eta_{p,\text{crit}} = 0.3562(6)$  [11, 12], while for  $f = 0.4$   $\eta_{c,\text{crit}} \approx 0.19$  and  $\eta_{p,\text{crit}}$  varies between 0.27 and 0.34 depending on  $R_{\text{dis}}/R_c$  [18]. In the interacting case instead, the colloid  $\eta_{c,\text{crit}}$  is approximately independent of  $f$ , while  $\eta_{p,\text{crit}}$  changes—it increases—with both  $f$  and  $R_{\text{dis}}/R_c$ . Note that a similar behavior is observed for the  $q$  dependence (at least, in the colloid regime) of  $\eta_{c,\text{crit}}$  and  $\eta_{p,\text{crit}}$  in the bulk [4]. In the AOV case,  $\eta_{p,\text{crit}}$  is essentially independent of  $q$ , while  $\eta_{c,\text{crit}}$  varies significantly with  $q$ . In the interacting-polymer case the opposite occurs:  $\eta_{p,\text{crit}}$  varies with  $q$ , while  $\eta_{c,\text{crit}}$  stays approximately constant.

In the AOV case we found [18] that colloids could undergo capillary condensation: for some values of the parameters, a colloid-gas phase in the bulk was in chemical equilibrium with a colloid-liquid phase in the matrix. In the present model no such phenomenon occurs unless one carefully tunes the system parameters.

The results we have presented rely on simulations of a very simplified model: first, we use a

CG model of the polymers in which each polymer is replaced by a monoatomic molecule; second, we use simplified potentials which allow us to reproduce correctly the thermodynamics in the low-density limit, but not the intermolecular distribution functions. An improvement of the model is clearly necessary if one wishes to obtain quantitatively accurate predictions. A multiblob model [25] in which polymers are represented as polyatomic molecules is necessary if one wishes to consider larger polymer-to-colloid ratios or to obtain accurate results for small values of  $R_{\text{dis}}/R_g$ . In the latter case, one would expect that an accurate modelling requires CG multiblob models in which the blob size is smaller than  $R_{\text{dis}}$ . Studies of the phase behavior of mixtures in random porous matrices with these improved models are not feasible with present computer resources. However, a less CPU-demanding task would be the study of the phase behavior in the presence of *regular* arrays of obstacles (the quenched colloids could belong to the sites of a regular lattice). Although less interesting from an experimental point of view (silica gels have a random distribution of pores) these type of systems could be more carefully studied, without relying on many different approximations. They can thus provide a theoretical laboratory, where one can understand the role of quenched obstacles on the phase behavior of these systems and thus develop theories that can then be extended to the more difficult random case. Work in this direction is in progress.

## Acknowledgments

It is a pleasure to thank Jean-Pierre Hansen for inspiring comments. The MC simulations were performed at the INFN Pisa GRID DATA center and on the INFN cluster CSN4.

- 
- [1] L. D. Gelb, K. E. Gubbins, R. Radhakrishnan, and M. Sliwinska-Bartkowiak, Rep. Prog. Phys. **62**, 1573 (1999).
  - [2] S. Asakura and F. Oosawa, J. Chem. Phys. **22**, 1255 (1954).
  - [3] A. Vrij, Pure and Appl. Chem. **48**, 471 (1976).
  - [4] P. G. Bolhuis, A. A. Louis, and J. P. Hansen, Phys. Rev. Lett. **89**, 128302 (2002).
  - [5] A. P. Gast, C. K. Hall, and W. B. Russell, J. Colloid Interface Sci. **96**, 251 (1983).



- [6] H. N. W. Lekkerkerker, W. C. K. Poon, P. N. Pusey, A. Stroobants, and P. B. Warren, *Europhys. Lett.* **20**, 559 (1992).
- [7] E. J. Meijer and D. Frenkel, *J. Chem. Phys.* **100**, 6873 (1994).
- [8] M. Dijkstra, J. M. Brader, and R. Evans, *J. Phys.: Condens. Matter* **11**, 10079 (1999).
- [9] M. Schmidt, H. Löwen, J. M. Brader, and R. Evans, *Phys. Rev. Lett.* **85**, 1934 (2000); *J. Phys.: Condens. Matter* **14**, 9353 (2002).
- [10] M. Dijkstra and R. van Roij, *Phys. Rev. Lett.* **89**, 208303 (2002).
- [11] R. L. C. Vink and J. Horbach, *J. Chem. Phys.* **121**, 3253 (2004).
- [12] R. L. C. Vink, J. Horbach, and K. Binder, *Phys. Rev. E* **71**, 011401 (2005).
- [13] M. Schmidt, E. Schöll-Paschinger, J. Köfinger, and G. Kahl, *J. Phys.: Condens. Matter* **14**, 12099 (2002).
- [14] R. L. C. Vink, K. Binder, and H. Löwen, *Phys. Rev. Lett.* **97**, 230603 (2006).
- [15] R. L. C. Vink, K. Binder, and H. Löwen, *J. Phys.: Condens. Matter* **20**, 404222 (2008).
- [16] G. Pellicane, R. L. C. Vink, C. Caccamo, and H. Löwen, *J. Phys.: Condens. Matter* **20**, 115101 (2008).
- [17] R. L. C. Vink, *Soft Matter* **5**, 4388 (2009).
- [18] M. A. Annunziata and A. Pelissetto, *Mol. Phys.* **109**, 2823 (2011).
- [19] P. G. de Gennes, *J. Phys. Chem.* **88**, 6469 (1984).
- [20] P. G. De Sanctis Lucentini and G. Pellicane, *Phys. Rev. Lett.* **101**, 246101 (2008).
- [21] T. Fischer and R. L. C. Vink, *J. Chem. Phys.* **134**, 055106 (2011).
- [22] C. N. Likos, *Phys. Rep.* **348**, 267 (2001).
- [23] A. A. Louis, P. G. Bolhuis, J. P. Hansen, and E. J. Meijer, *Phys. Rev. Lett.* **85**, 2522 (2000).
- [24] P. G. Bolhuis, A. A. Louis, J. P. Hansen, and E. J. Meijer, *J. Chem. Phys.* **114**, 4296 (2001).
- [25] See, e.g., C. Pierleoni, B. Capone, and J. P. Hansen, *J. Chem. Phys.* **127**, 171102 (2007), G. D’Adamo, A. Pelissetto, and C. Pierleoni, *Soft Matter* **8**, 5151 (2012), and references therein.
- [26] J. Dautenhahn and C. K. Hall, *Macromolecules* **27**, 5399 (1994).
- [27] P. G. Bolhuis and A. A. Louis, *Macromolecules* **35**, 1860 (2002).
- [28] A. Pelissetto and J.-P. Hansen, *J. Chem. Phys.* **122**, 134904 (2005).
- [29] A. Pelissetto and J. P. Hansen, *Macromolecules* **39**, 9571 (2006).
- [30] S. Caracciolo, B. M. Mognetti, and A. Pelissetto, *J. Chem. Phys.* **125**, 094903 (2006).

- [31] A. Pelissetto, J. Chem. Phys. **129**, 044901 (2008).
- [32] J. Zausch, P. Virnau, K. Binder, J. Horbach, R. L. C. Vink, J. Chem. Phys. **130**, 064906 (2009).
- [33] G. M. Torrie and J. P. Valleau, J. Comp. Phys. **23**, 197 (1977).
- [34] E. Marinari and G. Parisi, Europhys. Lett. **19**, 451 (1992).
- [35] E. Luijten, M. E. Fisher, and A. Z. Panagiotopoulos, Phys. Rev. Lett. **88**, 185701 (2002).
- [36] M. Hasenbusch, Phys. Rev. B **82**, 174433 (2010).
- [37] N. B. Wilding and A. D. Bruce, J. Phys: Condens. Matter **4**, 3087 (1992).
- [38] A. D. Bruce and N. B. Wilding, Phys. Rev. Lett. **68**, 193 (1992).
- [39] I. Bodnár and W. D. Oosterbaan, J. Chem. Phys. **106**, 7777 (1997).
- [40] S. M. Ilett, A. Orrock, W. C. K. Poon, and P. N. Pusey, Phys. Rev. E **51**, 1344 (1995).
- [41] R. Tuinier and C. G. de Kruif, J. Chem. Phys. **110**, 9296 (1999).
- [42] N. A. M. Verhaegh, J. S. van Duijneveldt, J. K. G. Dhont, and H. N. W. Lekkerkerker, Physica **230A**, 409 (1996).
- [43] R. Tuinier, P. A. Smith, W. C. K. Poon, S. U. Egelhaaf, D. G. A. L. Aarts, H. N. W. Lekkerkerker, and G. J. Fleer, Europhysics Lett. **82**, 68002 (2008).
- [44] References [4, 40, 43] do not report explicit estimates of the critical points. The numbers reported in Table II have been extracted from figures appearing in the original papers. The reported experimental estimates are obtained from Fig. 2(i) of Ref. [40] and from Fig. 1 of Ref. [43] (we assume  $\eta_{c,\text{crit}} = 0.2$  in both cases), the numerical results of Ref. [4] are taken from their Fig. 3.
- [45] G. J. Fleer and R. Tuinier, Adv. Colloid Interface Sci. **143**, 1 (2008).
- [46] The values of  $z_c$  at coexistence are quite large and correspond, in the hard-sphere case, to systems in the solid phase, i.e. such that  $\eta_c^r > \eta_{c,\text{solid}} = 0.545(2)$  [W. G. Hoover and F. H. Ree, J. Chem. Phys. **49**, 3609 (1968)]. We obtained  $\eta_c^r$  by solving the equation  $z_c R_c^3 = (z_c R_c^3)_{\text{coex}} f_H(\eta_c^r)$  where  $f_H(\eta_c^r)$  was obtained by using Hall's equation of state [K. R. Hall, J. Chem. Phys. **57**, 2252 (1972)]. The fugacity  $(z_c R_c^3)_{\text{coex}}$  at the liquid-solid coexistence was computed by using the Carnahan-Starling equation of state [N. F. Carnahan and K. E. Starling, J. Chem. Phys. **51**, 635 (1969), L. L. Lee, J. Chem. Phys. **103**, 9388 (1995)]:  $(z_c R_c^3)_{\text{coex}} = 3\eta_{c,\text{liq}}/(4\pi) \exp[f(\eta_{c,\text{liq}})]$  with  $f(\eta) = \eta(8 - 9\eta + 3\eta^2)/(1 - \eta)^3$  and  $\eta_{c,\text{liq}} = 0.494(2)$ .

- [47] M. E. J. Newman and G. T. Barkema, Phys. Rev. E **53**, 393 (1996).
- [48] A. K. Hartmann and A. P. Young, Phys. Rev. B **64**, 214419 (2001).
- [49] A. A. Middleton and D. S. Fisher, Phys. Rev. B **65**, 134411 (2002).
- [50] L. A. Fernandez, V. Martín-Mayor, and D. Yllanes, Phys. Rev. B **84**, 100408 (2011).